sustainability

MDPI

Article

Novel Copper Alginate Microspheres as Ecological Fungicides

Marko Vinceković [1,*], Slaven Jurić [1], Kristina Vlahoviček-Kahlina [1], Adrijana Novak [2], Dario Ivić [2], Laura Hazler [1], Tanja Jurkin [3], Arijeta Bafti [4] and Nataša Šijaković Vujičić [5]

1 Division of Agroecology, Department of Chemistry, Faculty of Agriculture, University of Zagreb, 10000 Zagreb, Croatia; sjuric@agr.hr (S.J.); kvkahlina@agr.hr (K.V.-K.); laura.hazler@gmail.com (L.H.)
2 Centre for Plant Protection, Croatian Agency for Agriculture and Food, Gorice 68b, 10000 Zagreb, Croatia; adrijana.novak@hapih.hr (A.N.); dario.ivic@hapih.hr (D.I.)
3 Radiation Chemistry and Dosimetry Laboratory, Ruđer Bošković Institute, Bijenička c. 54, 10000 Zagreb, Croatia; tjurkin@irb.hr
4 Faculty of Chemical Engineering and Technology, University of Zagreb, Trg Marka Marulića19, 10000 Zagreb, Croatia; abafti@fkit.unizg.hr
5 Division of Organic Chemistry and Biochemistry, Ruđer Bošković Institute, Bijenička c. 54, 10000 Zagreb, Croatia; natasa.sijakovic@irb.hr
* Correspondence: mvincekovic@agr.hr

Abstract: Phytopathogenic fungi are living organisms that cause plant diseases and great damage to agricultural products. Despite the wide range of commercial fungicide products in use, there is a clear need for new and environmentally friendly fungicides. Here we propose a new ecological fungicide, copper alginate microspheres prepared by ionic gelation. The microspheres were characterized (morphology and topography, encapsulation efficiency, loading capacity, swelling behavior, rheology, kinetics and mechanism of copper ions release) and their in vitro antifungal potential against selected genera of phytopathogenic fungi was evaluated. Copper alginate microspheres inhibited spore germination of *Botrytis cinerea*. Compared to the control, the inhibition of *B. cinerea* spore germination (48%) was greater than that of the commercial fungicide Neoram® (22%). The mycelial growth of *Cercospora beticola* and *Phytophthora ramorum* was also significantly inhibited by the addition of copper alginate microspheres. Novel fungicide offer effective disease control while minimizing environmental impact and promoting sustainable agriculture practices.

Keywords: encapsulation; copper alginate microspheres; ecological formulation; fungicides

Citation: Vinceković, M.; Jurić, S.; Vlahoviček-Kahlina, K.; Novak, A.; Ivić, D.; Hazler, L.; Jurkin, T.; Bafti, A.; Šijaković Vujičić, N. Novel Copper Alginate Microspheres as Ecological Fungicides. *Sustainability* **2024**, *16*, 5637. https://doi.org/10.3390/su16135637

Academic Editor: Antonio Zuorro

Received: 17 May 2024
Revised: 14 June 2024
Accepted: 22 June 2024
Published: 1 July 2024

1. Introduction

Phytopathogenic fungi are causal agents of plant diseases and represent probably the most diverse group of ecologically and economically relevant threats to plants [1]. Depending on the species, they parasitize almost all parts of the plant, especially when they find themselves in favorable conditions for development. Chemical or biological fungicides are used to control pathogenic fungi which can cause enormous losses in agricultural products. Fungicides are widely used, highly regulated, legitimate and useful tools that can provide significant benefits to agriculture. They can be effective in protecting crops, but at the same time can also have negative impacts on the environment (soil, water and air contamination) because many of them are organic pollutants [2]. To maximize fungicide benefits we need to use them safely and efficiently; misuse can cause negative ecological effects.

Despite the wide range of commercial fungicide products on the market, there is a clear need for new and innovative fungicides, due to the development of resistant fungal strains to fungicide active ingredients, regulatory limitations, increasing customer expectations, new diseases and their spread, and new environmental protection policies. The introduction of nanotechnology into agriculture can improve crop production by developing nano fertilizers and nano treatments for plant diseases [3,4], however, there

is not enough data in the literature on the efficacy and environmental impact of nano agrochemicals under field conditions [5].

Nowadays, a considerable number of phytochemical companies offer numerous and different classes of fungicides, where copper(Cu)-based fungicides play an important role due to their antifungal and antibacterial effects [6]. The major benefits of Cu-based compounds are the relatively high toxicity to plant pathogens, low cost, and low mammalian toxicity of the Cu compounds as well as their chemical stability and prolonged residual effects [7]. Cu is an essential micronutrient for plants and is an important component of fungicide and bactericide formulations on a global scale. Cu fungicides belong to the group of few fungicides that can be used in organic farming and still play an almost inevitable role in organic production, sustainable use of pesticides, and integrated pest management [8]. Cu compounds are protectant fungicides, which remain on the surface of the plant and are only effective before the pathogens infect the plant. They create a protective barrier on the surface of the plant, inhibiting the development of pathogens before penetrating the tissue. Cu ions interact with biochemical pathways in the pathogen in a non-specific manner, affecting many biochemical steps. Foliar application of copper fungicides enables the contact of Cu ions with germinating spores, creating enzyme systems that cause metabolic collapse and prevent further development of fungal cells [9]. The successful use of Cu-containing agents for the control of phytopathogenic plant diseases dates back more than 100 years, which can result in the accumulation of copper in the soil and negative ecological effects. Although Cu is a very important nutrient for living cells, as it is an integral part of many metalloenzymes, such as cytochrome c oxidase [10], it is known that it is phytotoxic at higher concentrations. In addition to phytotoxicity, the disadvantages are the development of Cu-resistant strains, soil accumulation and negative effects on soil biota as well as food quality parameters and regulatory pressure in agriculture worldwide, high concentrations of Cu salts in preparations, instability in field conditions and solubility in water [11]. To overcome the mentioned disadvantages, it is necessary to apply a new approach to the production of Cu fungicides, such as encapsulation. Encapsulation is an advanced technology by which solids, liquids, or gases may be loaded into a carrier matrix (usually biopolymeric microparticles within micro- or nano-scale) and allows controlled release. Microparticles loaded with an active substance (microparticle formulation) increase the stability of encapsulated active substance and reduce the amount required for application, but the most important role is the possibility of targeted and controlled release.

Numerous studies have pointed out that microparticles formed from sodium alginate (ALG) serve as valuable materials for encapsulating agents for various applications. ALG is a linear polysaccharide that easily forms a gel in the presence of multivalent cations under mild conditions due to the presence of alternating blocks of β-D-mannuronic acid (M units) and α-L-guluronic (G units) linearly linked by 1,4-glycosidic linkages [12]. The addition of divalent or trivalent cations to an aqueous solution of ALG causes immediate cross-linking and formation of an ALG hydrogel. The ability of ALG gel formation is widely used both in academia and industry for several applications. Some key applications of ALG gel formation are tissue engineering, wound healing, drug delivery, food industry, biotechnology and medical applications. The encapsulation of bioactive components in microparticles of ALG is a valuable tool in agriculture, especially in the nutrition and protection of plants [13,14].

Cu ions have a wide range of activity against bacteria, oomycetes and fungi interacting with nucleic acids, interfering with energy transport, disrupting enzyme activity, and affecting the integrity of cell membranes of pathogens. The primary mechanism of the antifungal effect of Cu ions is their uptake and physical deterioration of the membrane, which leads to the influx of Cu [15]. Following absorption into the fungus or bacterium, the Cu ions will link to various functional groups present in many proteins and disrupt their functions. Despite its wide spectrum, the sensitivity of different species of plant pathogens to Cu is variable. In testing of Cu-based fungicide formulations, different species of fungi, oomycetes or plant pathogenic bacteria should be selected. Suitable candidates for such

research are plant pathogens that are economically important and that have developed resistance to certain organic fungicides. Phytopathogenic fungi *Botrytis cinerea* Pers. and *Cercospora beticola* Sacc., and the oomycete (fungus-like organism) *Phytophthora ramorum* Werres et al. fulfil such criteria.

Botrytis cinerea is a filamentous fungal pathogen that causes gray mold disease [16]. It is a destructive and ubiquitous plant pathogen and parasitizes a large number of host plants (vegetables, fruits, ornamental flowers) causing severe economic losses in crops before and after harvest. Due to its high genetic variability [17], *B. cinerea* develops resistance to some chemical fungicides [18]. *Cercospora beticola* typically infects plants of the Amaranthaceae family (mainly sugar beet, spinach and swiss chard) causing *Cercospora* leaf spot (CLS) disease [19]. This pathogen is the most destructive foliar beet disease in warm and humid [20]. CLS can be managed by using fungicides, however, after repeated exposure, *C. beticola* becomes resistant to some active ingredients of fungicides [21]. *Phytophthora ramorum* is a filamentous, diploid oomycete, belonging to a group of organisms often known as 'water moulds'. It is an invasive pathogen that can cause extensive damage to more than 150 plant species, including some valuable forest trees [22]. Depending on the host, symptoms vary from leaf spot, blight, death of twigs, cancer and, finally, the death of a plant [23]. In coastal California and southern Oregon, *P. ramorum* causes sudden oak death, a disease that has killed millions of trees, primarily tanoak and coast live oak [24]. The most important host of *P. ramorum* in Europe is rhododendron. All three pathogens have developed resistance to important classes of fungicides in recent years. It should be emphasized that Cu-based compounds, although used for a long time, can be still effective in pathogen suppression [25].

In this work, copper alginate microspheres (ALG/Cu) were prepared by ALG ionic gelation and their potential as an ecological fungicide was evaluated. A preliminary set of experiments was performed to study the antifungal effect on selected phytopathogenic fungi (*Botrytis cinerea* and *Cerospora beticola* Sacc.) and the oomycete (fungus-like microorganism) *Phytophthora ramorum*.

2. Materials and Methods

2.1. Materials

Low viscosity sodium alginate (CAS Number: 9005-38-3; Brookfield viscosity 4–12 cps (1% in H_2O at 25 °C) purchased from Sigma Aldrich (Burlington, VT, USA) and copper sulfate pentahydrate (CAS Number: 7758-99-8) purchased from Gram-Mol d.o.o. (Zagreb, Croatia) were used for microsphere preparation. All other chemicals were of analytical grade and used as received without further purification.

2.1.1. Copper Alginate Microsphere Preparation

ALG/Cu were prepared by ionic gelation as previously described [13]. 100 mL of ALG solution (1.5%) was dropped into an equal volume of copper sulfate pentahydrate solution (2, 3, or 4%) through a size 120 µm nozzle at a vibration frequency of 2000 Hz and a pressure of 555 mbar (Encapsulator Büchi-B390, BÜCHI Labortechnik AG, Flawil, Switzerland). During preparation, the emerging microspheres (prepared at different initial concentrations of Cu: 8 mmol dm^{-3} (Sample 1), 12 mmol dm^{-3} (Sample 2) and 16 mmol dm^{-3} (Sample 3)) were mixed on a magnetic stirrer (IKA topolino, Staufen, Germany). ALG/Cu were formed in the cross-linking solution under mechanical stirring (MSH-300, Biosan; MM-540, Tehtnica, Železniki, Slovenia; Hei-Tec, Heidolph, Germany) for about 30 min to harden further, then filtered through a single-layer muslin and washed 3 times with distilled water to wash away excess $CuSO_4 \times 5H_2O$ and stored at 4 °C until further studies.

2.1.2. Preparation of Pathogens

The effect of ALG/Cu was assessed on three pathogens: *Botrytis cinerea*, *Cercospora beticola* and *Phytophthora ramorum*. Isolates, BC/7/19 (*B. cinerea*), CB/16/19 (*C. beticola*), PR/1/18 (*P. ramorum*), were obtained from the mycological collection of the Centre for

Plant Protection (Croatian Agency for Agriculture and Food, Zagreb, Croatia). For each isolate, separate plates were inoculated with a plug of mycelia cut from actively growing cultures. *B. cinerea* and *C. beticola* were inoculated on PDA (Potato dextrose agar, Biolife) while for *P. ramorum* carrot-pieces agar was used (CPA—50 g of cut carrot root pieces and 15 g of agar (Select Agar, Gram-Mol d.o.o., Zagreb, Croatia). Plates were incubated in separate growth chambers at 20 °C (*B. cinerea*, *C. beticola*) and 15 °C (*P. ramorum*) for seven to ten days. Prepared isolates were used further in the experiment.

2.2. Methods

2.2.1. Attenuated Total Reflectance Fourier Transform Infrared Spectroscopy (ATR-FTIR)

ALG/Cu samples were analyzed by Fourier transform infrared spectroscopy (FTIR) coupled with Attenuated Total Reflectance (ATR) recording technique. FTIR-ATR spectra of the samples were acquired using the Cary 660 FTIR spectrometer (Agilent Technologies, Palo Alto, CA, USA) and the Golden Gate single-reflection diamond ATR accessory (Specac). Spectra were recorded in the mid-infrared region (spectral range: 4000–400 cm^{-1}) and transmission mode. Details are given in S.2.2.1.

2.2.2. Physicochemical Characterization of Copper Alginate Microspheres

Encapsulation Efficiency, Loading Capacity and Swelling Degree

Detailed procedures for encapsulation efficiency (EE), loading capacity (LC) and swelling degree (S_w) determination are presented in Supporting Materials (S.2.2.2.1.). The concentration of Cu ions in the filtrate was determined by UV-VIS spectrophotometer (Shimadzu, UV-1700, Kyoto, Japan) at λ_{max} = 795 nm.

In Vitro Release of Cu Ions from Copper Alginate Microspheres

In vitro, the release of Cu ions from ALG/Cu was studied by dispersing 4 g of microspheres in 200 mL of deionized water and left to stand without stirring during experiments at room temperature. At appropriate time intervals, the dispersion was stirred for 60 s, aliquots were withdrawn and the concentration of Cu ions was determined by UV/VIS spectrophotometer (λ_{max} = 795 nm). Results are presented as the fraction of released Cu ions using the equation:

$$f_{Cu} = R_t/R_{tot}, \quad (1)$$

where f represents the fraction of released Cu^{2+}, R_t is the amount of Cu^{2+} released at time t and R_{tot} is the total amount of Cu^{2+} in microspheres.

Rheological Measurements

The rheological characteristics of microspheres were analyzed through oscillatory rheology. The storage (G′) and loss (G″) moduli were measured using a mechanical rheometer (MCR 302, Anton Paar, Stuttgart, Germany). The rheometer was equipped with a sandblasted steel plate−plate geometry (PP25/S, Anton Paar, Graz, Austria) and operated with a gap of 2 mm. The instrument was equipped with a true-gap system, and data were collected using RheoCompass software 1.33.540. Sandpaper was attached to the surface of the base plate to prevent the microspheres from slipping during the measurements. The sample temperature was regulated using a Peltier temperature control system located at the base of the geometry, supplemented by a Peltier-controlled hood (H-PTD 200). During the experiment, a sample was positioned on the rheometer's base plate, and the plate was adjusted using the true-gap function of the software. After allowing 2 min at 25 °C, measurements of G′ and G″ moduli were consistently taken within the linear viscoelastic region (LVR). The yield stress was determined by conducting a strain (γ) sweep between 0.01% and 100% at a constant frequency of 5 rad/s. The rheological properties of the sample were found to be strain-independent up to the yield strain. Beyond the yield strain, the rheological behavior became nonlinear. Subsequent frequency sweeps (0.1–100 rad/s) were carried out at 25 °C, maintaining a strain value of 0.1% within the LVR to explore the time-dependent deformation behavior of the sample.

2.2.3. Microscopic Observations

The morphology of ALG/Cu was analyzed by optical microscopy (OM) (Leica MZ16a stereo microscope, Leica Microsystems Ltd., Balgach, Switzerland), scanning electron microscope (SEM) (FE-SEM, model JSM-7000F, Jeol Ltd., Tokyo, Japan) and atomic force microscope (AFM) (Nanosurf CoreAFM, Nanosurf AG, Liestal, Switzerland).

The average diameter of wet and dry microspheres was determined by LM using Olympus Soft Imaging Solutions GmbH (version E_LCmicro_09Okt2009). Twenty microspheres were randomly selected from batches produced in triplicate, to determine the size distribution.

Samples for SEM analyses were placed on high-conductive graphite tape. FE-SEM was connected to an EDS/INCA 350 (energy dispersive X-ray analyzer) manufactured by Oxford Instruments Ltd. (Oxon, UK).

AFM images were taken using Nanosurf CoreAFM under ambient conditions. The non-contact mode was used for acquisition with a setpoint of 55% with Tap300Al-G tip with a nominal spring constant of 40 N/m, a tip radius less than 10 nm and a nominal resonant frequency of 300 kHz on a 10 × 10 μm surface with 0.78 s acquisition time. Images were processed with Nanosurf software 3.10.5. Surface roughness (Rq) is obtained by squaring each value of Z (height) in the sample and rooting the arithmetic mean of these values. Thus, the roughness is calculated as the arithmetic average of the absolute heights in the entire height line of the sample, so the presence of a smaller number of larger deviations can affect the roughness. Surface roughness was calculated on three different locations of the samples for better accuracy. Images were processed using the *Gwyddion* program v 1.4. [26].

Fungal spore morphology was analyzed by optical microscope OM and SEM. Spores of *B. cinerea*, *C. beticola* and *P. ramorum* were dispersed in distilled water before observation under OM and dried before examination under SEM. The average diameter of spores was determined by OM.

2.2.4. The Electrostatic Charge and Size of Fungal Spores Suspended in Water and Copper Ions Solutions

Dynamic light scattering (DLS) measurements for the determination of hydrodynamic diameter of nanoparticles in synthesized suspensions were performed using Zetasizer Ultra (*Malvern Panalytical, London United Kingdom*), equipped with a 632.8 nm He-Ne laser, using the Multi-Angle Dynamic Light Scattering (MADLS®) technology. MADLS performs analysis at three different scattering angles (front 13°, side 90°, back 173°) and compiles the data into a single integrated measurement. (To naravno, ako ćeš prikazati rezultate MADLS mjerenja, ako ne onda uobičajeno, samo back-scatter mjerenja).

The measurements were performed using DTS0012 1 cm plastic cuvettes. Each measurement consisted of 5 runs with at least 30 subruns. Hydrodynamic diameters were calculated based on intensity, volume and number distributions and the results are presented as the mean values of 3–5 measurements each performed at three angles. Zeta potential measurements were performed on the same instrument, using electrophoretic light scattering in DTS1070 folded capillary cells. The values of zeta potential are given as the mean value of three measurements. Zetasizer Ultra (Malvern Panalytical) was purchased by the project UIP-2017-05-7337 financially supported by the Croatian Science Foundation.

2.2.5. Testing the Antifungal Effect of Copper Alginate Microspheres

Effect of Copper Alginate Microspheres on *B. cinerea* Conidia Germination

1 g of ALG/Cu (Sample 1, Sample 2 or Sample 3) was suspended in a 10 mL Falcon tube filled with sterile water. Conidia were scraped from sporulating colonies of *B. cinerea* isolates with a sterile toothpick and transferred to a prepared Falcon tube. 1 mL of suspension was evenly poured onto PDA plates in three replicates and placed in a growth chamber at 20 °C and 60% relative humidity for incubation. PDA plates with 5% of the commercial fungicide Neoram® (copper oxychloride 37.5% wettable granules) and distilled water were used as a reference for comparison. Suspension with distilled water was used as an untreated control.

Germination and elongation of the germ tube (30 germ tubes were measured for each sample) have been monitored and measured with an Olympus BX53 optical microscope 18 h after incubation. Measurements were performed using the CellSens Dimension program V 2.3. (Olympus Hamburg, Germany). Based on the average length values of the germ tubes in control and those incubated with ALG/Cu or commercial fungicide, inhibition of spore germination was quantified according to Abbott's relation [27].

Antifungal Effect of Alginate Copper Microspheres on Mycelium Growth of *C. beticola*

A suspension of ALG/Cu and *C. beticola* conidia was prepared as described for *B. cinerea*. 1 mL of a suspension was evenly poured onto PDA plates in three replicates and placed in a growth chamber at 28 °C and 80% relative humidity for incubation. After 7 days of incubation, the number of developed colonies was read using a millimeter grid divided into 4 squares. Based on the number of developed colonies in control and those incubated with ALG/Cu, inhibition of mycelial growth was quantified according to Abbott [27].

Antifungal Effect of Copper Alginate Microspheres on Infestations of *Rhododendron* sp. Leaves by *P. ramorum*

10 g of ALG/Cu were placed in Petri dishes with a diameter of 120 mm. 100 mL of spring water, two pieces of mycelial disc of *P. ramorum* and two leaves of *Rhododendron* sp. were added to each Petri dish. The control Petri dishes contained 100 mL of spring water, two mycelial discs of *P. ramorum* and two leaves of *Rhododendron* sp. The experiment was set in two replicates at room temperature to encourage the formation of sporangia. Visual observations and results were read after two weeks. The presence of sporangia and zoospores in the water and on the *Rhododendron* leaves was examined with an Olympus BX53 microscope. Symptoms of leaves infection were also recorded by visual observation.

Data Analysis

All experiments were repeated three times. and the data was presented with mean values and standard deviations. Data corresponding to a normal distribution were analyzed by one-way analysis of variance (One-way ANOVA) and differences between treatments were evaluated by the Tukey test ($p \leq 0.05$) in the statistical program SPSS, version 27 (IBM SPSS Statistics IBM, Corp., New York, NY, USA, 2023).

3. Results and Discussion

The results are presented and discussed in two sections. In the first section, the important ALG/Cu physicochemical properties are analyzed. In the second part, the potential of antifungal activity of ALG/Cu against pathogens (*B. cinerea*, *C. beticola* and *P. ramorum*) is evaluated.

3.1. Copper Alginate Microsphere Physicochemical Properties

3.1.1. Identification of Interactions between Microsphere Constituents

The functional groups characterizing the bulk chemistry of the ALG/Cu were identified by FTIR. The spectra of ALG as well as ALG/Cu prepared at lower concentrations of Cu ions were described previously [28]. Characteristics of the ALG spectrum are a strong broadband assigned to the stretching modes of hydroxyl groups (–OH) around 3300 cm^{-1}, pyranoid ring C–H stretching at 2925 cm^{-1}, very sharp stretching at 1595 cm^{-1} and medium sharp stretching at 1405 cm^{-1} corresponding to vibrations of asymmetric and symmetric carboxylate groups (COO^{-}), weak broad stretching vibration at 1295 cm^{-1} assigned to C–O group. Bands situated around 1026 cm^{-1} are attributed to the ALG saccharide structure. The characteristic peaks of copper sulfate pentahydrate are at 3200, 1667, 1067 and 860 cm^{-1}. A broad stretching frequency at 3200 cm^{-1} and a band of medium intensity at 1667 cm^{-1} represent the bending modes of the hydroxyl group, while frequencies at 1067 and 860 cm^{-1} are characteristic bands of inorganic sulfates ($(SO_4)^{2-}$ stretching region [29]. The comparison between spectra of ALG and ALG/Cu showed the most

significant changes in the ALG functional groups region: hydroxyl (OH), ether (COC) and carboxylate (COO^-). The intensities of the main ALG peaks in the spectrum of ALG/Cu are reduced and shifted towards lower or slightly higher wave numbers. Shifting of the ALG broad band around 3300 cm^{-1} indicates Cu ion's interaction with hydroxyl groups while shifting the peaks of carboxylate stretching vibrations arose from the Cu ions binding to oxygen atoms from negatively charged and uncharged carboxyl groups [30]. In comparison with calcium ions [31], the band assigned to the asymmetric elongation vibration of COO^- was more downshifted with Cu ions, thus confirming that the alginate chains interacted more effectively with Cu ions [28]. The affinity of Cu^{2+} to alginate chains is ten times higher than that of Ca^{2+} [32].

Figure 1 shows the effect of Cu ion concentrations on the spectrum of ALG/Cu. There are no significant changes in the intensity of the absorption band around 3300 cm^{-1} between Samples 1 and 2, however, Sample 3 spectrum shows broadening and more intense stretching vibrations suggesting enhanced intermolecular hydrogen bonds. With an increase in the concentration of Cu ions, the intensities of asymmetric and symmetric carboxylate stretching vibrations follow the order of Sample 2 < Sample 1 < Sample 3 indicating a change in the intensity of interaction between ALG carboxylate groups and Cu ions. Small changes in the intensity of carboxylate stretching vibrations, as well as a certain irregularity of changes about the increase in the concentration of Cu ions, indicate a complex change in the cross-linking of alginate chains. During gelation of ALG, Cu cations interact with the functional groups forming a cross-linked network of alginate chains. Unlike calcium ions, which crosslink alginate chains only electrostatically, crosslinking with Cu ions occurs mainly by coordination of covalent bonds and partially by ionic bonds [33].

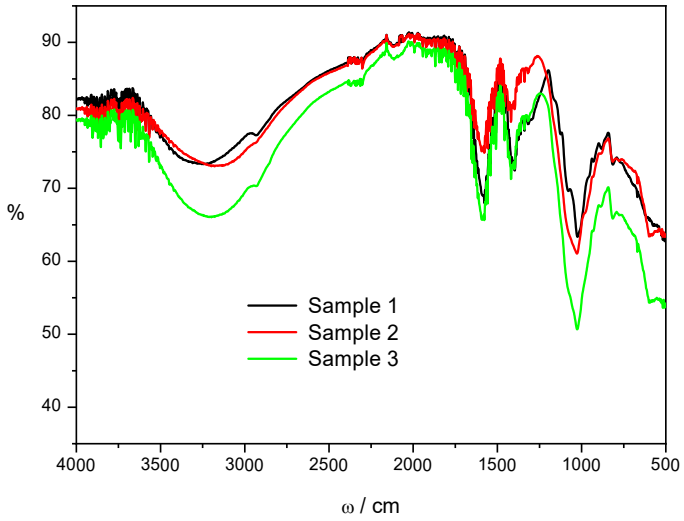

Figure 1. FTIR spectra of ALG/Cu microspheres prepared at initial Cu concentration: 8 mmol dm^{-3} (Sample 1), 12 mmol dm^{-3} (Sample 2) and 16 mmol dm^{-3} (Sample 3).

The weak bands at 1080 cm^{-1} and strong peaks at 1026 cm^{-1} are assigned to the C=O and C-C bonds of guluronic and mannuronic units, respectively [34]. It can be seen that the intensity of the strong peak at 1026 cm^{-1} assigned to mannuronic units increases significantly with the amount of Cu cations loaded in the microspheres. Unlike calcium-induced gelation of ALG, which is mainly based on cross-linking between ions and uronates, Cu ions bind to mannuronic and guluronic alginate units [35]. The weak band at 1080 cm^{-1} assigned to guluronic units can be seen only for Sample 1 and disappeared at higher concentrations of Cu ions. Papageorgiou et al. [36] proposed in the metal-alginate complexes a "pseudo-bridged" unidentate coordination with intermolecular hydrogen bonds in polyguluronic regions and the bidentate bridging coordination in the polymannuronic region.

Changes in spectra clearly show small structural differences in microspheres prepared at different concentrations of Cu ions. Similarly was observed by Omidian et al. [37]

who suggested that bands concerning carboxylate groups can be used to follow structural changes of different alginate gels.

3.1.2. Morphology of Copper Alginate Microspheres

Prepared microspheres were almost spherical and colored blue due to the presence of Cu ions. The size of wet microspheres was 120 ± 16 µm regardless of the initial Cu concentration. After drying to a constant mass, the shape and size of the microspheres changed significantly, they became irregular and smaller. During drying, the size of the ALG/Cu decreases by approximately 46%. The surface morphology of microspheres is presented in Figure 2. The surfaces became wrinkled with the appearance of more or less intertwined threads due to the loss of water and moisture associated with the stress relaxation processes of biopolymers [38]. Different morphologies seen in Figure 2 are a reflection of structural differences in the gel network. The smoothest surface of Sample 3 points to weaker intermolecular forces with a fewer number of crosslinking points between two alginate molecules [39]. The crosslinking density influences how much water the gel can absorb. Lower crosslinking density generally leads to higher swelling [40]. In the investigated concentration range of Cu ions, S_w increased from 35.10 ± 2.27%, 59.93 ± 3.31% to 90.95 ± 5.72% indicating a decrease in crosslinking density from Sample 1 to 3.

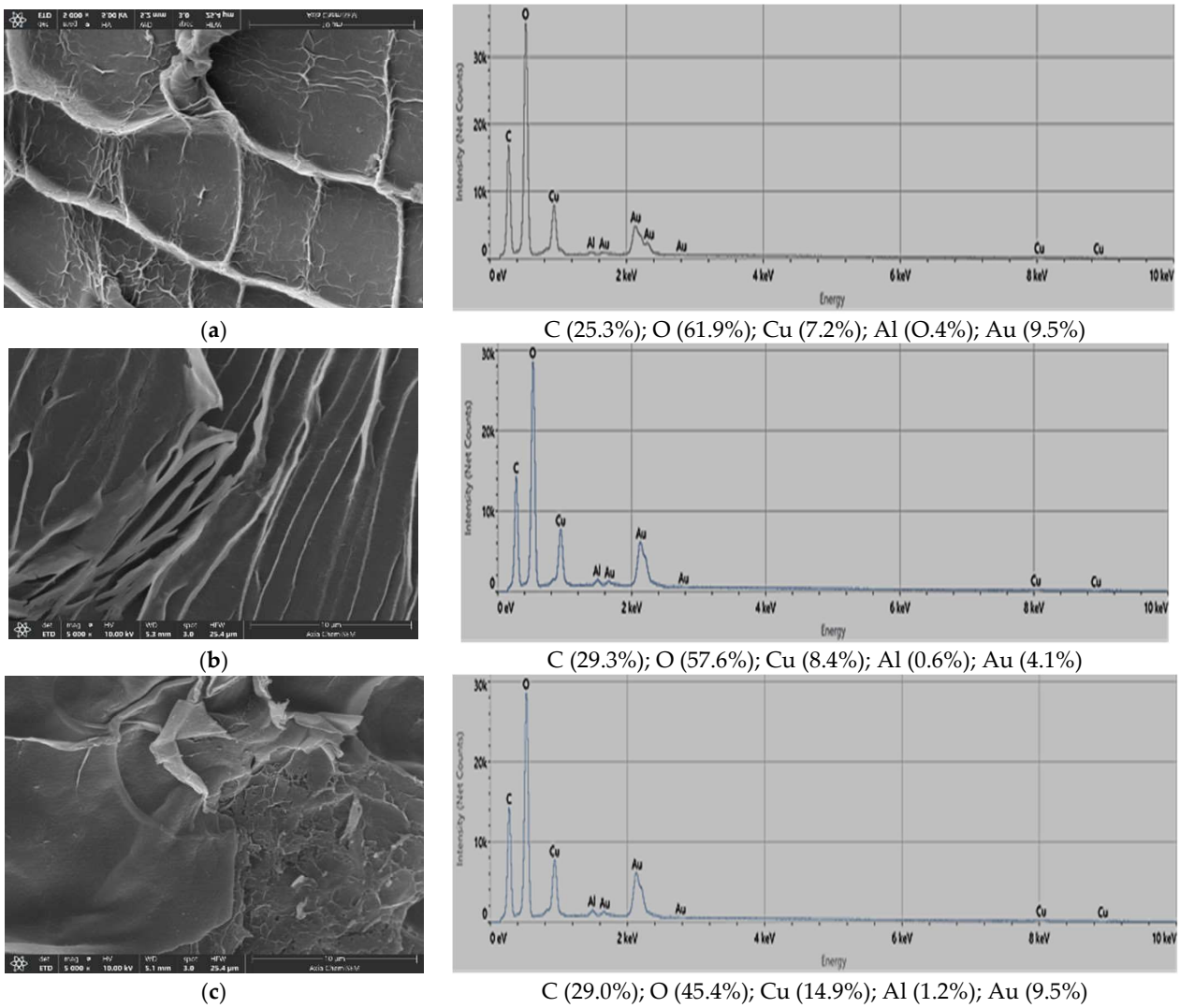

Figure 2. SEM microphotographs of ALG/Cu (**a**) Sample 1, (**b**) Sample 2 and (**c**) Sample 3. Bars are indicated. The EDS analysis (expressed as atomic weight percentage) of the surface layers is shown on the right side next to the corresponding microspheres.

EDS spectral analysis of the surface layers (the electron probe can penetrate to a depth of about 1 µm) is shown in Figure 2 on the right side next to the corresponding image of ALG/Cu. The major elements are oxygen, carbon, and copper. The amount of Cu on the surface increases from 7.2 ± 0.1, 8.4 ± 0.1 to 14.9 ± 0.1% following the increase in the amount of initial concentration of Cu ions used during the preparation of microspheres. The samples do not contain a sodium atom due to complete ion exchange with Cu ions during the cross-linking process. Detected amounts of aluminum and gold are probably residues of compounds used during the sample preparation for analysis.

AFM imaging was done at a few different regions of each microsphere to ensure the accuracy of the obtained results. In Figure 3, the topography of each sample can be seen, along with a 3D topography view with a corresponding Z-axis scale (i.e., height). As can be seen, the surfaces consist of stacked granular particles. By increasing the content of Cu ions in the microspheres, the grains become smaller, but the overall surface becomes less rough. The grain height was between 30 and 100 nm, which could be seen in the smallest images (lowest row in Figure 3). As can be seen in Figure 3, the grains at Sample 1 were the largest and elongated, forming a rougher surface. Determined surface roughness values are presented in Table 1. The values are observed by calculating the average of five roughness values obtained at different locations on the sample.

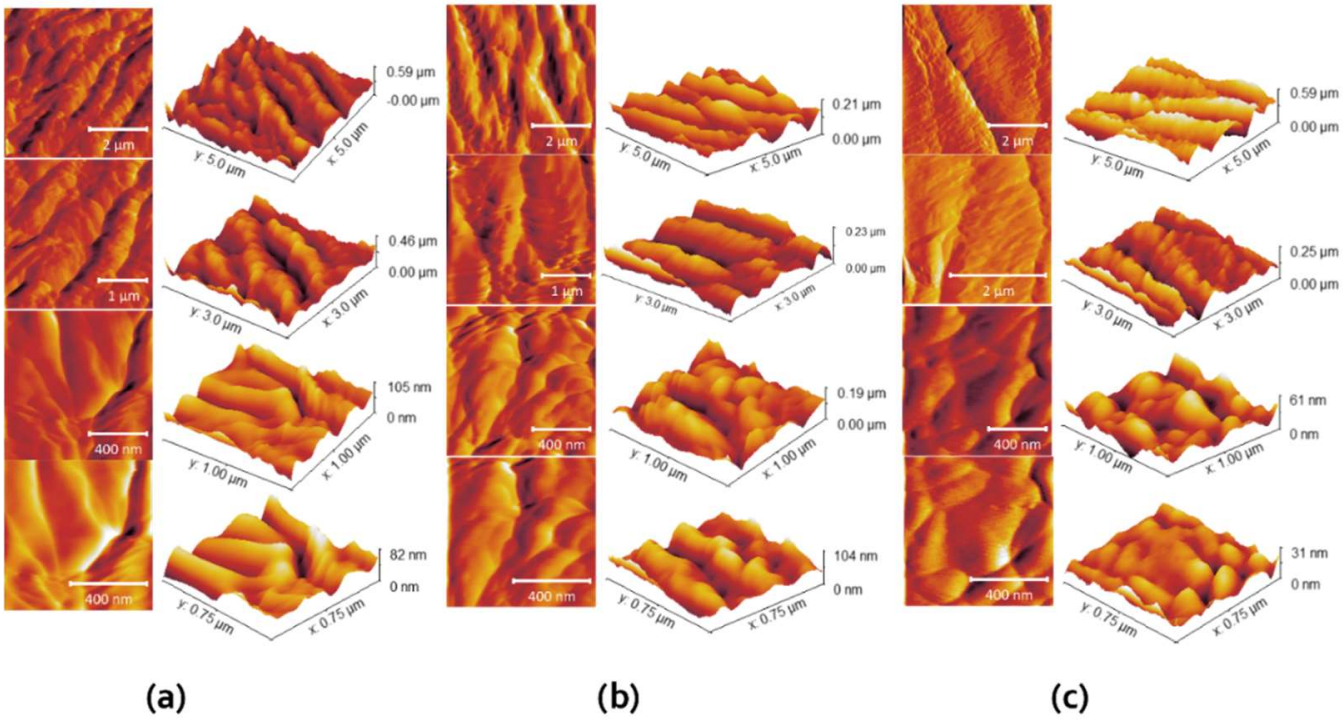

Figure 3. AFM micrographs of analyzed samples-top view of 2D-height data and 3D—height data of (**a**) Sample 1, (**b**) Sample 2, and (**c**) Sample 3, from top to down presented higher magnifications.

Table 1. Surface roughness values determined for ALG/Cu prepared at initial Cu concentration: 8 mmol dm^{-3} (Sample 1), 12 mmol dm^{-3} (Sample 2) and 16 mmol dm^{-3} (Sample 3); average roughness (R_a), root mean square of roughness (R_q).

ALG/Cu	Ra/nm	Rq/nm
Sample 1	23.89	29.45
Sample 2	18.04	20.68
Sample 3	3.99	5.44

An important step in the foliar application of Cu-based fungicides is adhesion to the plant surface due to the possible blowing of microspheres from the leaves by wind or rain.

Surface roughness is an important property of microspheres due to their ability to adhere to other substrates [41]. It was shown that higher surface roughness reduces adhesion in real contact [42], which indicates some advantages of Sample 3 over Sample 1 or Sample 2 (Table 1). The smallest roughness parameters of Sample 3 indicated a better adhesion ability in comparison with other samples. Adhesion enables the contact of Cu ions with germinating spores and creates enzyme systems that prevent the further development of cells and mycelium [22].

3.1.3. Rheological Properties of Copper Alginate Microspheres

The rheological properties of microspheres correlate with their microstructures providing useful information for maintaining their stability during processing and application. The results of the dynamic oscillation test gave information concerning the influence of Cu ion concentrations on the structure, and mechanical and thermal properties.

Amplitude Sweep

The viscoelastic properties of the ALG/Cu were characterized using oscillatory rheology. The storage modulus G′ (Pa) represents the elastic component of the viscoelastic behavior, indicating the solid-like properties of the sample. Typically, the elastic component (G′) predominates over the loss modulus or viscous component (G″) under low applied shear, reaching a plateau within the linear viscoelastic region (LVR). The linear viscoelastic region encompasses the range where applied stress minimally influences the 3D structure of the material. The point at which the linear relationship between stress and strain is disrupted is known as the yield point, signaling a change in the material's structure. During the amplitude test, the frequency is kept constant while varying the shear strain. Strain (γ) sweep tests were performed within a strain range of γ = 0.01 to 100% at an angular frequency of ω = 5 rad s^{-1} and a temperature of 25 °C. The values of G′ and G″ remained nearly unaffected by the applied strain up to 0.8%. The results of the amplitude sweep are shown in Figure S1 (Supplementary Material).

The rheological behavior of the microspheres prepared with different initial Cu concentrations exhibited similar viscoelastic properties. As the concentration of Cu in microspheres increased the elastic modulus decreased in the order Sample 1 > Sample 2 > Sample 3 (Table 2). Following the decrease of the elastic modulus, the shear stress has also decreased in the same order. Yield point values of Samples 1, 2 and 3 were 1334 Pa, 1249 Pa and 1173 Pa, respectively. As the yield stress values decreased the yield strain values increased in the same order from 3.5% to 5.2%. Data obtained indicate a somewhat softer but still well-organized structure of Sample 3. This is particularly noticeable in the assessment of the loss factor.

Table 2. Results of amplitude sweep tests of ALG/Cu prepared at initial Cu concentration: 8 mmol dm^{-3} (Sample 1), 12 mmol dm^{-3} (Sample 2) and 16 mmol dm^{-3} (Sample 3) examined at 25 °C.

ALG/Cu	G′ (max)/Pa	Yield Point Stress/Pa	Yield Point Strain/%	Flow Point/Pa	Loss Factor	Flow Transition Index
Sample 1	39,075	1334	3.5	2170	0.17	1.63
Sample 2	35,700	1249	4.8	2015	0.18	1.61
Sample 3	31,117	1173	5.2	1721	0.17	1.47

The loss factor, defined as $\tan(\delta) = G''/G'$, indicates the relative elasticity of viscoelastic materials. A material with a tan(δ) value less than 1 is considered to be in a solid state. The material with a value of tan(δ) lower than 1 is in the solid state. The material with a value of tan(δ) = 0.1 belongs to a stiff one and is indicative of well-ordered systems. The loss factor values determined in the examined cases were 0.17–0.18. The flow transition index represents a measure of the yielding zone, a valley between a yield point and a flow point.

The value of the flow transition index is similar for Sample 1 and 2, and somewhat lower for Sample 3.

The storage modulus values, yield point, flow point, and flow transition index follow a decreasing order from Sample 1 > Sample 2 > Sample 3. However, it is noteworthy that despite the variation in Cu concentration, all investigated samples demonstrated high elastic modulus (G′) values in the order of 10^4 Pa. This suggests the formation of a well-ordered and elastic structure, even at the microspheres prepared at 16 mmol dm^{-3} Cu concentration.

Frequency Sweep

Frequency sweep analysis characterizes the time-dependent response of a sample within a non-destructive deformation range, providing insights into the behavior and internal structure of polymers. Conducting frequency sweep studies ($\omega = 0.1-100$ rad/s at 0.2% strain, LVR) on the examined samples at 25 °C revealed that throughout the frequency range, the storage modulus (G′) values consistently exceeded the loss modulus (G″) values (G′ > G″). This indicates a prevailing elastic nature rather than a viscous character for the samples, as shown in Figure 4. The frequency-dependent evolution of G′ and G″ for all investigated samples was observed. At higher frequencies, the investigated samples showed higher rigidity reflected in higher G′ values. The gradual rise in elastic modulus with frequency suggests the presence of relaxation processes, potentially induced by the release of reversible entrapped entanglements or the opening of intermolecular junctions [43]. In general, the elastic modulus of alginate polymer depends on the number of cross-links, as well as the length and stiffness of the chains between the cross-links [44]. Since the storage modulus dependence of frequency is very similar for all investigated samples prepared at different Cu concentrations we assume a similar structural microsphere arrangement, although a slightly lower value of the elastic modulus of Sample 3 indicated a somewhat looser network structure.

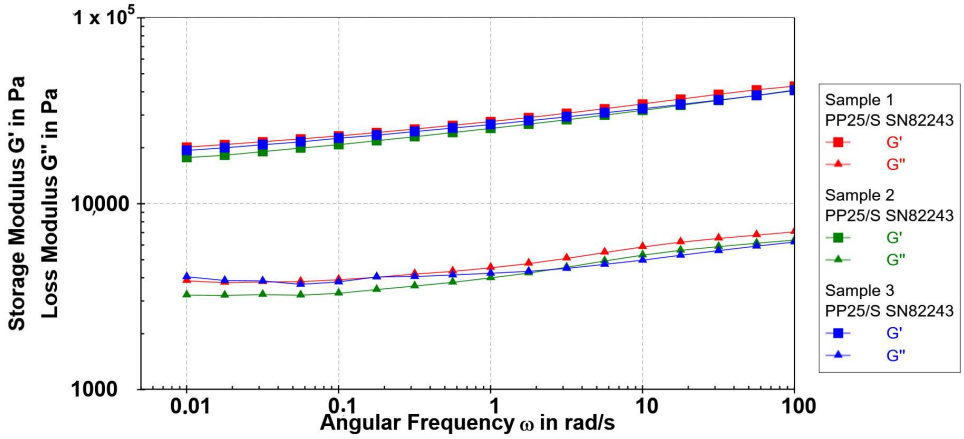

Figure 4. Frequency sweep test (G′ (■) and G″ (▲) values) of Sample 1 (red), Sample 2 (green), and Sample 3 (blue) at a strain of 0.1% and 25 °C.

The low angular frequency (ω) region is regarded as highly sensitive to changes in the polymer network structure. In the higher frequency range, Samples 1 to 3 exhibited a range of loss factor (tan δ) values from 0.15 to 0.17, while in the low-frequency range, the tan δ values were slightly higher, ranging from 0.18 to 0.21. Notably, only Sample 3, showed a subtle change in tan δ from 0.15 to 0.21 at very low frequencies. Although the structural strength and rigidity of cross-linked polymers are slightly influenced by the Cu concentration, the relative elasticity (tan δ) is well-maintained across the entire frequency range. Frequency sweep measurements demonstrated that the microspheres remained stable over an extended period, regardless of the Cu concentration.

Temperature Sweep

To identify the thermal behavior of the microcapsules an oscillatory temperature sweep was performed. This involved an investigation at a constant strain and frequency but changing the temperature. This allowed us to determine phase angle data and temperatures at which structural change occurred.

Samples 1–3 were subjected to a temperature sweep till 80 °C during oscillatory measurements to determine the softening properties of the samples with different Cu concentrations. The value of complex viscosity (η^*) decreased with increasing temperature for all examined samples (Figure S2, Supplementary Material). Throughout the entire temperature range, the complex viscosity exhibited the following sequence: Sample 1 > Sample 2 > Sample 3.

Samples 1–3 exhibited the phase shift angle (φ) of 7.5° at 15 °C, indicating a solid behavior at low temperatures. Upon heating, the elastic component decreased, as shown by the transition to a higher phase angle. There were differences between the elasticity of the samples after heating to 80°, with Sample 3 tending towards the less elastic due to the highest phase angle (19.3°) than Sample 2 with 18.5°, and Sample 1 as the most solid-like due to the lowest phase angle (14.6°). The onset of significant viscosity and elasticity change occurred at 65 °C for all the samples. The loss factor (tan δ) was 0.14 at 15 °C, while at 80 °C, it ranged from 0.25 to 0.35. The data obtained from the temperature sweep indicate the thermal stability of the investigated samples with a slight decrease in elasticity with an increase in the Cu content.

3.1.4. In Vitro Copper Ions Release from Copper Alginate Microspheres

The release of a bioactive component from a hydrophilic microparticle may involve different types of physicochemical processes, including wetting, swelling (penetration of solution into the matrix), polymer stress relaxation (transition from glassy to rubbery state), diffusion through the matrix, disintegration, dissolution, or erosion of the structure, or their combination [45]. Understanding the mechanism and kinetics of bioactive components released from microspheres is critical for the optimal development of formulations for a specific application. Bearing in mind the main factors (concentration of biopolymer and gelling cation, microsphere preparation technique, chemical composition and geometry of microspheres) that influence the release of bioactive components [13,46], we prepared ALG (Cu at a constant concentration of ALG and different concentrations of Cu ions. The release profiles of Cu ions from all three types of ALG/Cu are presented in Figure 5.

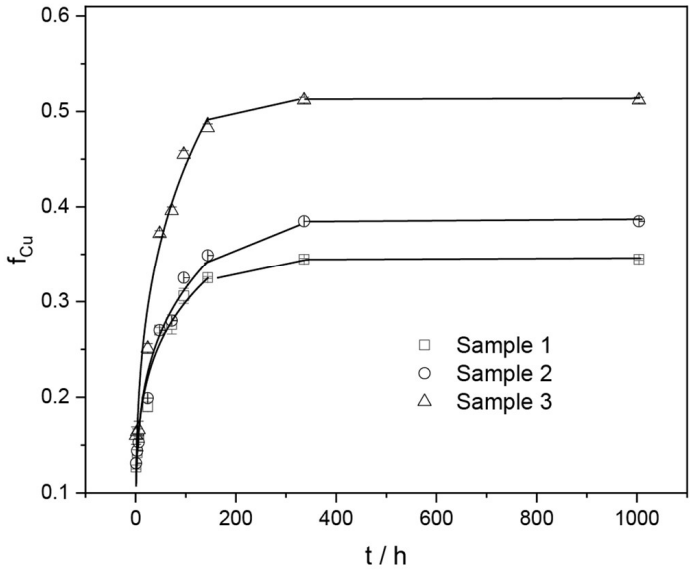

Figure 5. Fraction of released Cu (f_{Cu}) with time (t) from ALG/Cu prepared at initial Cu concentration: 8 mmol dm^{-3} (Sample 1), 12 mmol dm^{-3} (Sample 2) and 16 mmol dm^{-3} (Sample 3). The error bars indicate the standard deviation of the means.

All release profiles are characterized by a rapid initial release followed by a slower release obeying the power law equation. The highest amount of released copper ions was detected in Sample 3. This may simply be attributed to the fact that microspheres have higher Cu loading capacity (LC values ranged from 2.08 ± 0.0011 to 2.28 ± 0.0012 to 2.8 ± 0.0041 mmol for 1.0 g of ALG/Cu prepared with Cu concentration from 8, 12 to 16 mmol dm^{-3}, respectively) as well as the weakest crosslinking density between alginate strands. Results were analyzed using a simple empirical Korsmeyer-Peppas model [47]

$$f_{Cu} = k\, t^n, \quad (2)$$

where f_{Cu} is a fraction of released Cu ions, k is a kinetic constant characteristic of a specific system taking structural and geometrical aspects into account, n is the release exponent representing the release mechanism, and t is the release time.

According to Korsmeyer–Peppas, the release exponent n can be characterized by three different mechanisms (Fickian diffusion, anomalous (non-Fickian diffusion), or Type II transport). Values of $n < 0.43$ indicate the release is controlled by classical Fickian diffusion, $n > 0.85$ is controlled by Type II transport, involving polymer swelling and relaxation of the polymeric matrix, whereas values of n between 0.43 and 0.85 show the anomalous transport kinetics determined by a combination of the two diffusion mechanisms and Type II transport. Table 3. represents variations of the release constant, exponent n and correlation coefficient of Cu ions released from ALG/Cu prepared at different initial concentrations of Cu.

Table 3. Variation of the release constant (k/h^n), exponent (n) and correlation coefficient (R^2) of Cu released from ALG/Cu prepared at different initial Cu concentrations: 8 mmol dm^{-3} (Sample 1), 12 mmol dm^{-3} (Sample 2) and 16 mmol dm^{-3} (Sample 3).

ALG/Cu	*k*	*n*	R^2
Sample 1	0.164 ± 0.018	0.13 ± 0.012	0.9975
Sample 2	0.180 ± 0.009	0.13 ± 0.010	0.9931
Sample 3	0.233 ± 0.025	0.14 ± 0.015	0.9987

According to the used model, n values lower than 0.45 revealed that the process of Curelease is controlled by diffusion and is closely related to the process of swelling. Thanks to the extremely strong ALG/Cu affinity, an incomplete Cu dissolution profile occurs over a time range longer than 24 h. Because of the hydrophilic nature of Cu cross-linked ALG/Cu, processes such as dissolution, diffusion and erosion also play a role in the release of Cu ions [48]. The increase in the release constant k with the initial concentration of copper cations is related to the differences in the structure of the microspheres, i.e., with the cross-linking density. A higher degree of swelling indicates a lower cross-linking density, which causes a higher rate of Cu ions release and is consistent with previous research [13]. It can be concluded that Sample 3 not only has a higher Cu loading but also releases a larger amount of Cu ions at a faster rate.

3.2. Antifungal Effect of Copper Alginate Microspheres on B. cinerea C. beticola and P. ramorum

3.2.1. Fourier Transformed Infrared (FTIR-ATR) Spectroscopy of *B. cinerea*, *C. beticola* and *P. ramorum* Mycelium

Figure 6 shows a typical fungal spectrum: broad absorption band between 3000 to 2800 cm^{-1}, characteristic bands for fatty acid, amide I and II (1700–1500 cm^{-1}), polysaccharides (1200–900 cm^{-1}) and the range between 700–900 cm^{-1} specific for the identification of microorganisms (the fingerprint region). Fungi infrared spectra reveal bands that are unique to particular functional groupings of biological origins as was shown by Mularczyk-Oliwa et al. [49]. In all spectra, the peak intensities decrease in the order *C. beticola* < *B. cinerea* < *P. ramorum* with a small shift towards higher or lower wave numbers. Peaks of broad bands appearing between 3000 to 3500 cm^{-1} consistent with O-H bond stretch-

ing are shifted in the same order; from 3269 to 3275 to 3362 cm^{-1}. This range might be caused by water molecules in the cytoplasm or extracellular water, such as moisture in the air.

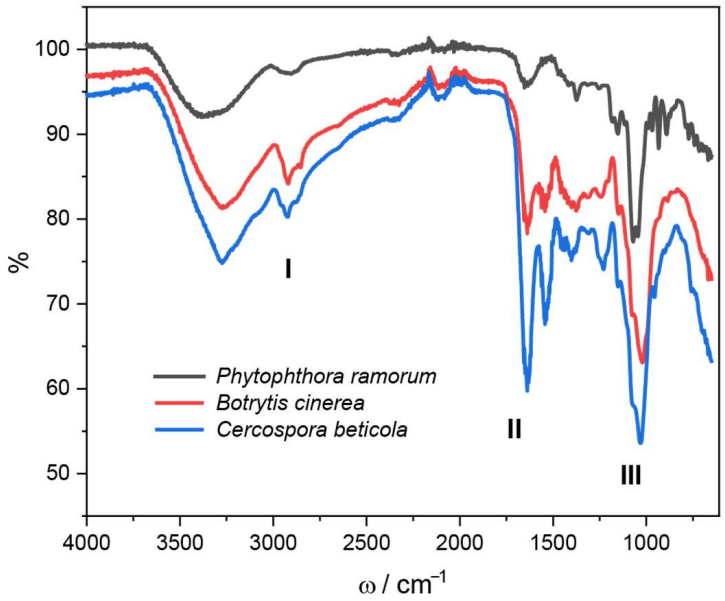

Figure 6. FTIR spectra of fungal mycelium: *P. ramorum* (black line), *B. cinerea* (red line) and *C. beticola* (blue line). Regions attributed to fatty acids (I), amide I and II (II) and polysaccharides (III) are denoted.

The region between 3000 and 2800 cm^{-1} shows the C-H stretching vibrations of CH_3 and CH_2 functional groups in fatty acid chains of various membranes. The spectra of *C. beticola* and *B. cinerea* are similar with peaks at 2926 cm^{-1}, while the peak of *P. ramorum* is shifted to 2905 cm^{-1}. The stretching vibrations of C=O, C-N, and the bending mode of NH in amide I are shown in the next area, from 1800 to 1500 cm^{-1}, as are the C-N stretching vibrations and bending mode of NH in amide II [50]. Sharp stretching and medium sharp stretching at 1640 and 1539 cm^{-1} (*C. beticola*) and at 1631 and 1540 cm^{-1} (*B. cinerea*) correspond to protein vibrations as well as vibrations of other fungal constituents [51]. In this region, *P. ramorum* shows only stretching at 1650 cm^{-1}.

In the region 1500–1200 cm^{-1}, the total absorbance is lower, although several different peaks are visible. This region is a mixed region that exhibited C=O symmetric stretching vibrations of COO^- functional groups of amino acid side chains or free fatty acids, CH_2 bending mode of lipids and proteins, and P=O asymmetric stretching vibrations in phospholipid head groups.

In the meanwhile, the symmetric stretching vibration of PO_2^- groups in nucleic acids and the C-O-C, C-O, and C-O-P stretching vibrations of different oligo and polysaccharides are proven in the area between 1200 and 900 cm^{-1} [52]. The strongest peaks corresponding to chitin vibrations are at 1032 cm^{-1} (*C. beticola*), 1026 cm^{-1} (*B. cinerea*) and 1031 cm^{-1} (*P. ramorum*) [53]. In the fingerprint region (700–900 cm^{-1}) [54] *C. beticola and B. cinerea* show similar spectra with lower total absorbance. Spectrum of *P. ramorum* mycelium exhibits several peaks corresponding to β-glucans (vibrations at 891 and 773 cm^{-1}) [55].

3.2.2. Morphological Properties of *B. cinerea*, *C. beticola* and *P. ramorum* Spores and Mycelium

Optical microphotographs of pathogen spores suspended in distilled water and SEM images of dryed spores are presented in Figure 7. The conidia of *B. cinerea* are ellipsoidal to ovoid with an approximate size of 14.72 ± 0.13 µm (Figure 7a) which is consistent with literature data [56]. Microphotograph of *C. beticola* (Figure 7c) reveals a needle-like and colorless conidia approximately 43.25 ± 12.184 µm in size which is consistent with previous descriptions [57]. *P. ramorum* sporangia are approximately 23.26 ± 2.87 µm in size and ellipsoid (Figure 7e) which is consistent with literature data [58].

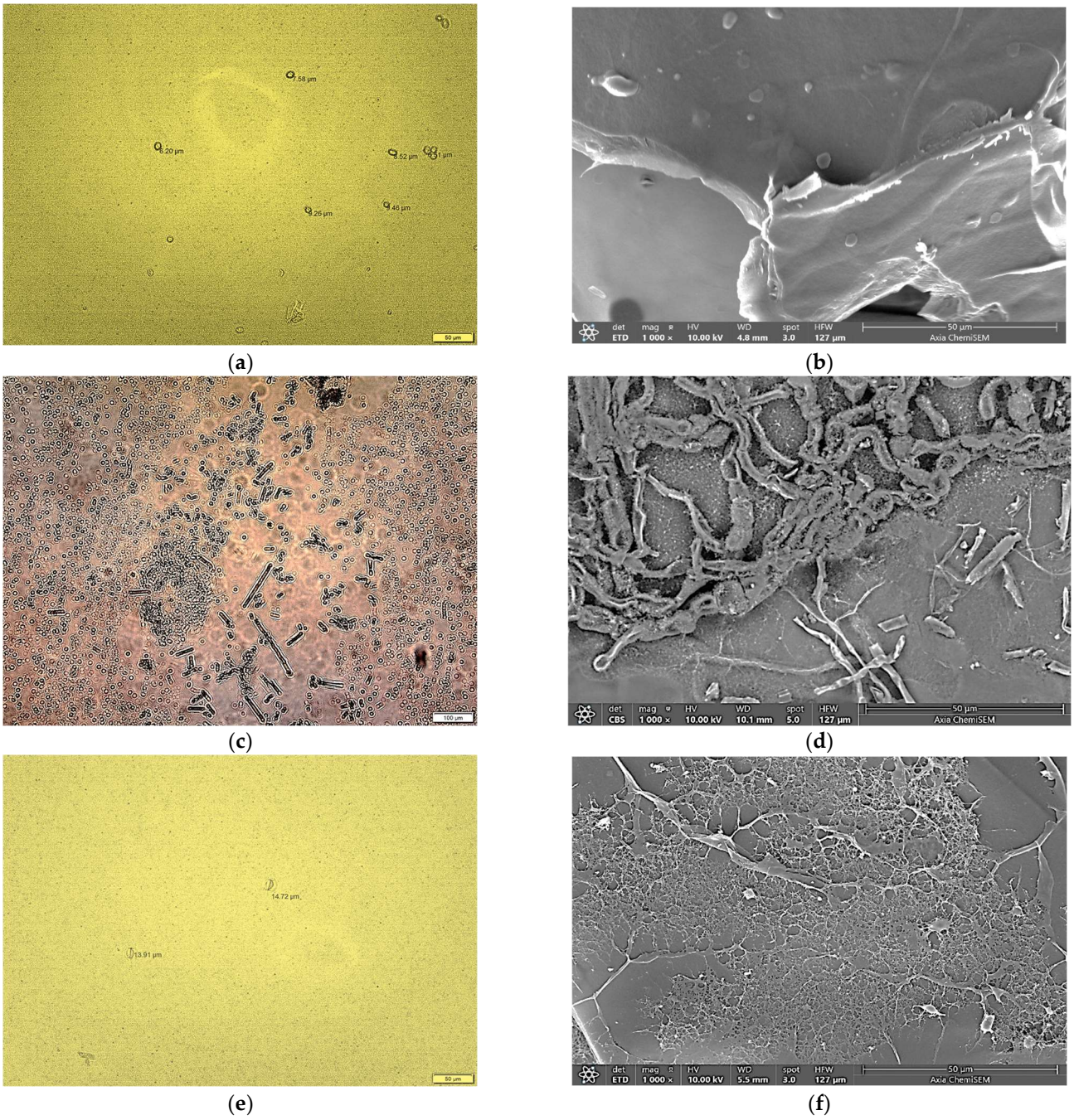

Figure 7. Microphotographs of (**a**) *B. cinerea*, (**c**) *C. beticola* and (**e**) *P. ramorum* spores obtained by optical microscope (OM) and (**b**) *B. cinerea*, (**d**) *C. beticola* and (**f**) *P. ramorum* spores, condiospores and hyphae obtained by scanning electron microscope (SEM). Bars are indicated.

SEM characterization revealed noticeable microstructural differences between three plant pathogenic species. The Microphotograph of *B. cinerea* shows a tapered apical dome of hypha with a smooth surface, ellipsoidal conidia, conidiophore and hyphae (Figure 7b). SEM characterization revealed noticeable microstructural differences between *C. beticola* and *P. ramorum*. *C. beticola* shows the presence of straight to flexuous conidia, and loosely arranged hyphae (Figure 7d). Pseudo-fungi *P. ramorum* exhibit thinner but densely packed hyphae (Figure 7f) compared to those of *C. beticola* forming a network structure.

EDS elemental mapping of the investigated plant parasites provides spatial distribution and elemental composition on the surface of mycelia (Figure S3, Supplementary Material). The spatial distribution of the most abundant elements in the surface layer is presented in the left

colon. All identifiable elements are listed in the tables to the corresponding images. The detected amount of Au is probably a residue after sample preparation for analysis.

3.2.3. Influence of Copper Ion Concentrations on the Electrostatic Charge and Size of Fungal Spores

The microbial cell is the natural adsorbent for metal ions due to its nature and the composition of the cellular membrane. The cell walls of fungi are generally composed of chitin, chitosan, β-glucans and mannan [59]. In addition, cell walls may contain lipids, protein, acid phosphatase, α-amylase, protease, melanin, and inorganic ions such as phosphorus, calcium, and magnesium [60]. The cell wall of oomycetes is different than in fungi, containing polysaccharides such as cellulose and other β-glucans [61]. Filamentous fungi accumulate metal ions into their mycelium and spores via mechanisms involving the fungal cell wall (intracellular/biosorption and extracellular/adsorption processes), which is also important for their survival and performance, as well as energetic uptake and valence conversion [62,63]. The influence of different concentrations of Cu cations on spores suspended in water was examined with a microscope, as well as by measuring the spore size, charge and zeta potential. The microscopic observation clearly shows the effects of Cu ions concentration on the number of single spores, that is the increase in Cu ions concentration resulted in their aggregation. Aggregation in submerged cultures of filamentous fungi depends on the surface charge of spores [64].

An important parameter describing the behavior of the solid-liquid interface charge is zeta potential. It is the electric potential of the shear plane in the electric double layer of a moving particle, and it is related to the particle surface charge. The surface charge of the fungal spore wall depends on the available functional groups. The relatively high negative zeta potential of all spores suspended in distilled water (-26.24 ± 0.63 mV for *B. cinerea*; -28.98 ± 1.3 mV for *C. beticola*; -23.07 ± 1.59 mV for *P. ramorum*) is in line with FTIR data and analysis of the relationship between relative surface hydrophobicity and surface electric charge [65]. The surface coating on top of the cell wall plays a crucial part in the electrostatic nature of the investigated species. The negative charge arises from various functional groups such as carboxyl, hydroxyl, amine and phosphate [66]. With increasing Cu ions concentration, fungal spores became less negatively charged due to the electrostatic binding of Cu cations (Figure 8a). The negative value of the zeta potential decreased as the concentration of copper ions increased. All spores maintained their negative charge even at greater Cu concentrations. Zeta potential is often used to explain the aggregation of microbial cells. At a lower concentration where the greatest changes in the zeta potential were observed, the size of measured particles was significantly changed (Figure 8b). The increase of copper cation concentration resulted in the aggregation of spores.

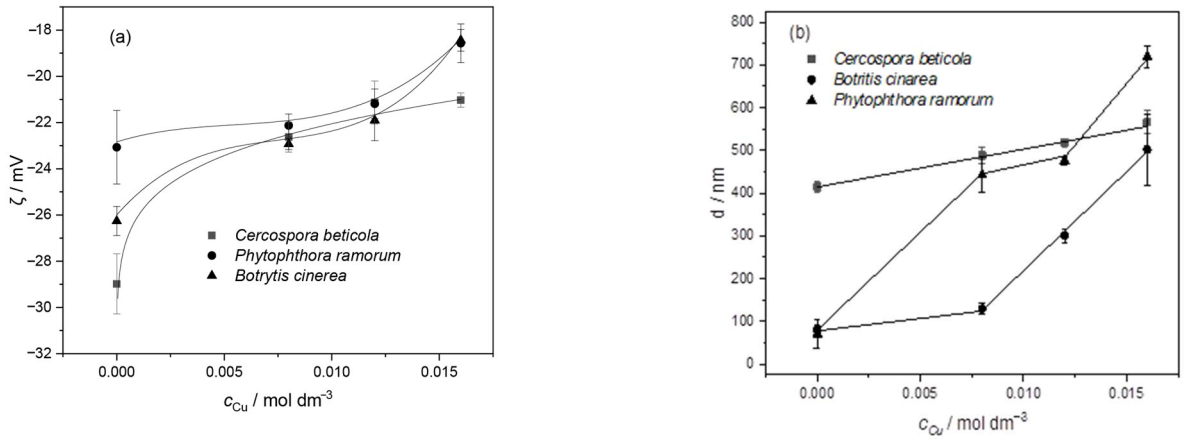

Figure 8. Variation of (**a**) the average zeta potential (ζ) and (**b**) the mean hydrodynamic diameter (d) of suspended fungal spores with Cu cation concentration (c_{Cu}/mol dm^{-3}). The error bars indicate the standard deviation of the means.

3.2.4. Antifungal Effect of Copper Alginate Microspheres on *B. cinerea*, *C. beticola* and *P. ramorum*

Antifungal Effect of Copper Alginate Microspheres on *B. cinerea*

Copper alginate microspheres prepared with different initial concentrations of Cu were used to evaluate the antifungal effect on *B. cinerea* isolates (Table 1). In addition to the easy formation of microspheres the advantage of alginate is its antimicrobial effect against various bacteria [67]. The results showed that copper alginate microspheres affect the length of the germ tube of *B. cinerea* and have the potential to control disease in the early stages of crop growth. This is consistent with the finding that Cu binds to the surface of *B. cinerea* spores during germination and slows it down [68,69].

Conidial germination of *B. cinerea* was verified if the germ tube length was equal to or greater than the conidia length [69]. After incubation, the lengths of the germ tubes were measured. Germ tube length measurement data are listed in Table 3. Figure S4 (Supplementary Material) shows the length of germ tubes measured in the control and in Sample 3. The results showed that three tested copper alginate samples inhibited conidial germination. The percentage of inhibition (I) was calculated as follows

$$I\ \% = ((L_c - L_{Cu})/L_c)\ x\ 100, \quad (3)$$

where L_c is the average length of the germ tube in control and L_{Cu} is the average length of the germ tube in treatment.

The inhibitory effect of copper alginate microspheres on *B. cinerea* increased with increasing concentration of Cu incorporated in ALG/Cu. The smallest germ tube length measured with Sample 3 reveals 48% inhibition which is even higher than with the commercial fungicide, Neoram® (inhibition 22%) in Table 4.

Table 4. Length (µm) of germ tubes after conidia incubation during 18 h in distilled water (control), treated with ALG/Cu (Samples 1, 2, 3) and fungicide Neoram® (5%).

n	Control	Sample 1	Sample 2	Sample 3	Neoram
1	32.70	16.32	54.55	41.21	40.81
2	56.20	13.64	24.39	24.96	39.78
3	27.36	40.99	64.84	30.29	76.43
4	35.85	18.81	25.84	8.25	6.80
5	27.61	3.40	33.66	55.42	53.57
6	42.81	54.56	21.08	9.89	27.31
7	16.88	19.78	26.33	8.16	45.10
8	38.99	30.33	51.07	17.88	26.62
9	31.15	19.72	30.92	23.80	23.94
10	66.73	8.88	32.33	14.49	26.81
11	54.25	11.37	55.29	52.46	31.25
12	15.04	38.08	33.26	16.25	21.17
13	33.01	38.15	67.43	6.00	42.59
14	77.46	32.68	46.33	25.86	19.49
15	16.88	24.70	15.12	22.37	45.90
16	50.36	11.44	35.85	15.73	59.02
17	24.46	82.32	50.10	10.20	16.93
18	32.97	63.17	46.83	18.54	23.41
19	33.20	48.29	31.79	23.65	50.34
20	39.49	108.87	4.96	16.29	26.72
21	43.68	48.03	66.35	9.40	16.88
22	77.77	36.13	37.77	29.89	52.15
23	73.12	19.52	20.44	26.65	38.75
24	50.13	22.18	19.24	24.46	37.10
25	45.73	31.25	42.06	38.77	30.22
26	41.71	55.40	62.78	18.52	31.47
27	59.30	11.44	41.11	18.60	19.69
28	42.68	21.34	79.34	37.09	38.73
29	91.29	42.08	44.75	19.88	29.34
30	61.76	48.30	21.40	28.97	44.36
Inhibition		23%	12%	48%	22%

Antifungal Effect of Copper Alginate Microspheres on *C. beticola*

The number of *C. beticola* colonies in the control and samples treated with ALG/Cu was counted. Data are listed in Table 5.

Table 5. The average number of colonies (at 2 cm^2) in the control and with ALG/Cu.

Sample	Number of Colonies				Average
Control	2	2	1	0	1.25
Control	2	2	0	2	1.50
Control	3	3	1	0	1.75
Sample 1	1	1	0	0	0.50
Sample 1	1	2	0	0	0.75
Sample 1	0	0	0	0	0.00
Sample 2	0	0	0	0	0.00
Sample 2	1	0	0	0	0.25
Sample 2	1	1	1	1	1.00

The relative percentage of developed colonies (inhibition percentage) was calculated based on the ratio between control and copper alginate microspheres. The percentage of inhibition was calculated as follows:

$$I\ \% = ((X - Y)/X)\ x\ 100, \quad (4)$$

where X is the average number of colonies on the control sample and Y is the average number of colonies on samples treated with copper alginate microspheres. Inhibition percentages of 61% for Sample 1 and 72% for Sample 2 revealed they are effective in preventing the development of *C. beticola* colonies. The Cu release inhibits the activity of fungal spores to prevent germination and provide a protective barrier against plant pathogens by covering plant surfaces [70].

Antifungal Effect of Copper Alginate Microspheres on *P. ramorum*

The effectiveness of ALG/Cu on *P. ramorum* was evaluated by visual observation of color changes in control solutions and solutions with samples treated with ALG/Cu, as well as by examination of infection symptoms characteristic of *P. ramorum* on rhododendron leaves. Visual inspection revealed the most pronounced color change in the control Petri dishes (Figure 9a). The presence of mycelia was confirmed by microscopy (Figure 9b). In Petri dishes with ALG/Cu, the color change was weaker indicating slower mycelial growth.

(**a**) (**b**)

Figure 9. (**a**) The control with *P. ramorum* and rhododendron leaves and (**b**) microphotograph of *P. ramorum* mycelium (20x magnification).

The presence of mycelia and a large number of sporangia and zoospores on the control leaves was confirmed with a microscope (Figure 10a). Mycelia, sporangia, and zoospores

did not develop on most leaves treated with ALG/Cu, although some leaves showed infection symptoms characteristic of *P. ramorum* (Figure 10b). Only a few and mostly empty and deformed sporangia were observed.

(**a**) (**b**)

Figure 10. Leaves of *Rhododendron* sp. (**a**) incubated for 7 days in water (control) and (**b**) with Samples 1, 2 and 3.

The obtained results revealed that copper alginate microspheres inhibited the development of *P. ramorum* mycelium. As already mentioned with the fungus *B. cinerea* and *C. beticola*, the microspheres can be used alone or as an addition to other fungicides.

4. Concluding Remarks

We have used a multi-technique approach to investigate physicoshemical properties of ALG/Cu prepared at various Cu ion concentrations and their antifungal potential.

Molecular interactions between Cu and ALG, microspheres morphology and topography, Cu amount in microspheres, swelling behavior and Cu ions release from microspheres depend on Cu ions concentration.

Rheological tests showed the formation of ordered and elastic structures that are mechanically and thermally stable regardless of the concentration of Cu ions in ALG/Cu. All microspheres have a similar structural arrangement, although the slightly lower value of the elastic modulus of those prepared with the highest concentration of copper indicates a slightly looser network structure.

Microspheres prepared at the highest Cu concentration have the highest Cu loading capacity, the smoothest surface, the highest swelling ability, and the weakest crosslinking density between alginate strands, and release a larger amount of Cu ions at a faster rate.

The prepared microspheres are designed to deliver Cu ions at a specific time and place providing longer protection against fungal infections. The targeted application of microspheres reduces the total amount of Cu ions needed. The mechanism that controls the release rate from microspheres is diffusion through the microsphere.

Copper alginate microspheres can persist on plant surfaces which is an important step in the foliar application of Cu-based fungicides. The smallest roughness parameters indicated a better adhesion ability of microspheres prepared at the highest concentration of Cu ions compared to other samples.

The morphological analysis of the selected pathogens followed literature descriptions (conidias of *B. cinerea* are ellipsoid to ovoid, *C. beticola* needle-like, and sporangia of *P. ramorum* ellipsoidal).

FTIR analysis of *B. cinerea*, *C. beticola* and *P. ramorum* revealed a typical fungal spectrum with characteristic functional groups (fatty acids, amides I and II, polysaccharides and specific fingerprint region).

The negative charge of the fungal spore wall arises from various functional groups (carboxyl, hydroxyl, amine and phosphate). The addition of Cu ions reduced the negative value of zeta potential and induced the aggregation of spores.

In vitro experiments revealed new microspheres as potential fungicides against phytopathogenic fungi. Cu ions release affected the conidial germination of *B. cinerea* and the mycelial growth of *C. beticola* and *P. ramorum*.

Among the advantages of copper alginate microspheres compared to traditional fungicides in the control of plant diseases are an environmentally acceptable and cost-effective production method, but the most important advantages are the slow release of Cu ions and a potentially longer duration of action. The periods between treatments and the number of treatments can be shortened, and the protection can be longer. With further research, the new copper alginate microspheres can be used as natural, ecological fungicides in the process of protecting plant crops from several important fungal diseases.

Supplementary Materials: The following supporting information can be downloaded at: https://www.mdpi.com/article/10.3390/su16135637/s1, Figure S1. Amplitude sweep tests (G′ (■) and G″ (▲) values) of Sample 1 (red), Sample 2 (green), and Sample 3 (blue) were determined at a constant angular frequency of 5 rad/s at 25 °C. Figure S2. Temperature sweep measurements of Sample 13 represented as (a) complex viscosity and (b) storage (G′) and loss (G″) modulus dependence determined at a constant strain 0.1% and a frequency of 1 Hz in a temperature range 1580 °C. Figure S3. Energy-dispersive spectroscopy (EDS) element mapping images of mycelium (a) *B. cinerea* (C, O, Au and K distribution) (b) *C. beticola* (C, O, N and K distribution) and (c) *P. ramorum* (C, O, Au and Na distribution) and elemental analysis (expressed in the atomic weight percent) using dispersive X-ray spectroscopy. Bars are indicated. Figure S4. Length of *B. cinerea* germ tubes after incubation for 18 hours in (a) control and (b) with ALG/Cu (Sample 3) at 20x magnification. References [71,72] cited in main.

Author Contributions: M.V.: conceptualization, methodology, writing original draft, project management and funding acquisition; S.J.: conceptualization, supervision, and editing; D.I. and A.N. review and editing; L.H., K.V.-K., A.B., T.J. and N.Š.V.: formal analysis. All authors have read and agreed to the published version of the manuscript.

Funding: Hrvatska Zaklada za Znanost: UIP-2014-09-6462.

Institutional Review Board Statement: Not applicable.

Informed Consent Statement: Not applicable.

Data Availability Statement: Dataset available on request from the authors.

Conflicts of Interest: The authors declare no conflicts of interest.

References

1. Doehlemann, G.; Ökmen, B.; Zhu, W.; Sharon, A. Plant pathogenic fungi. *Microbiol. Spectr.* **2017**, *5*, 703–726. [CrossRef] [PubMed]
2. Tudi, M.; Li, H.; Li, H.; Wang, L.; Lyu, J.; Yang, L.; Tong, S.; Yu, Q.J.; Ruan, H.D.; Atabila, A.; et al. Exposure Routes and Health Risks Associated with Pesticide Application. *Toxics* **2022**, *10*, 335. [CrossRef] [PubMed]
3. Wang, P.; Lombi, E.; Zhao, F.J.; Kopittke, P.M. Nanotechnology: A New Opportunity in Plant Sciences. *Trends Plant Sci.* **2016**, *21*, 699–712. [CrossRef] [PubMed]
4. Pariona, N.; Mtz-Enriquez, A.; Sanchez-Rangel, D.; Carrion, G.; Paraguay-Delgado, F.; Rosas-Saito, G. Green-synthesized copper nanoparticles as a potential antifungal against plant pathogens. *RSC Adv.* **2019**, *9*, 18835. [CrossRef] [PubMed]
5. Kah, M.; Kookana, R.S.; Gogos, A.; Bucheli, T.D. A critical evaluation of nanopesticides and nanofertilizers against their conventional analogues. *Nat. Nanotechnol.* **2018**, *13*, 677–684. [CrossRef] [PubMed]
6. Rusjan, D. Copper in Horticulture. In *Fungicides for Plant and Animal Diseases*; Dhanasekaran, D., Thajuddin, N., Panneerselvam, A., Eds.; Intec Open: London, UK, 2012; Chapter 13; pp. 257–278. [CrossRef]
7. Lamichhane, J.R.; Osdaghi, E.; Behlau, F.; Kohl, J.; Jones, J.B.; Aubertot, J.N. Thirteen decades of antimicrobial copper compounds applied in agriculture. A review. *Agron. Sustain. Dev.* **2018**, *38*, 28. [CrossRef]
8. La, T.A.; Iovinom, V.; Caradonia, F. Copper in plant protection: Current situation and prospects. *Phytopathol. Mediterr.* **2018**, *57*, 201–236. [CrossRef]
9. Plante, S.; Normant, V.; Ramos-Torres, K.M.; Labbé, S. Cell-surface copper transporters and superoxide dismutase 1 are essential for outgrowth during fungal spore germination. *J. Biol. Chem.* **2017**, *292*, 11896–11914. [CrossRef] [PubMed]

10. Chen, J.; Jiang, Y.; Shi, H.; Peng, Y.; Fan, X.; Li, C. The molecular mechanisms of copper metabolism and its roles in human diseases. *Pflugers Arch. Eur. J. Physiol.* **2020**, *472*, 1415–1429. [CrossRef] [PubMed]
11. Rehman, M.; Liu, L.; Wang, Q.; Saleem, M.H.; Bashir, S.; Ullah, S.; Peng, D. Copper environmental toxicology, recent advances, and future outlook: A review. *Environ. Sci. Pollut. Res.* **2019**, *26*, 18003–18016. [CrossRef] [PubMed]
12. Varaprasad, K.; Jayaramudu, T.; Kanikireddy, V.; Toro, C.; Sadiku, E.R. Alginate-based composite materials for wound dressing application. A mini review. *Carbohydr. Polym.* **2020**, *236*, 116025. [CrossRef] [PubMed]
13. Vinceković, M.; Jalšenjak, N.; Topolovec-Pintarić, S.; Đermić, E.; Bujan, M.; Jurić, S. Encapsulation of Biological and Chemical Agents for Plant Nutrition and Protection: Chitosan/Alginate Microcapsules Loaded with Copper Cations and *Trichoderma viride*. *J. Agric. Food Chem.* **2016**, *64*, 8073–8083. [CrossRef] [PubMed]
14. Vinceković, M.; Jurić, S.; Vlahoviček-Kahlina, K.; Martinko, K.; Šegota, S.; Marijan, M.; Krčelić, A.; Svečnjak, L.; Majdak, M.; Nemet, I.; et al. Novel Zinc/Silver Ions-Loaded Alginate/Chitosan Microparticles Antifungal Activity against *Botrytis cinerea*. *Polymers* **2023**, *15*, 4359. [CrossRef] [PubMed]
15. Salah, I.; Parkin, I.O.; Allan, E. Copper as an antimicrobial agent: Recent advances. *RSC Adv.* **2021**, *11*, 18179. [CrossRef] [PubMed]
16. Elad, Y.; Vivier, M.; Fillinger, S. Botrytis, the Good, the Bad and the Ugly. In *Botrytis—The Fungus, the Pathogen and Its Management in Agricultural Systems*; Fillinger, S., Elad, Y., Eds.; Springer: Cham, Switzerland, 2016; pp. 1–15. [CrossRef]
17. De Miccolis, A.; Pollastro, S.; Faretra, F. Genetics of *Botrytis cinerea*. In *Botrytis—The Fungus, the Pathogen and Its Management in Agricultural Systems*; Fillinger, S., Elad, Y., Eds.; Springer: Cham, Switzerland, 2016; pp. 433–455. [CrossRef]
18. Notte, A.M.; Plaza, V.; Marambio-Alvarado, B.; Olivares-Urbina, L.; Poblete-Morales, M.; Silva-Moreno, E.; Castillo, L. Molecular identification and characterization of *Botrytis cinerea* associated to the endemic flora of semi-desert climate in Chile. *Curr. Res. Microb. Sci.* **2021**, *2*, 100049. [CrossRef] [PubMed]
19. CABI. *Cercospora beticola* (Cercospora Leaf Spot of Beets). Invasive Species, Compendium. 2022. Available online: https://www.cabidigitallibrary.org/doi/10.1079/cabicompendium.12191 (accessed on 16 July 2022).
20. Rangel, L.I.; Spanner, R.E.; Ebert, M.K.; Pethybridge, S.J.; Stukenbrock, E.H.; de Jonge, R.; Secor, G.A.; Bolton, M.D. *Cercospora beticola*: The intoxicating lifestyle of the leaf spot pathogen of sugar beet. *Mol. Plant Pathol.* **2020**, *21*, 1020–1041. [CrossRef] [PubMed]
21. Kumar, R.; Mazakova, J.; Ali, A.; Sur, V.P.; Sen, M.K.; Bolton, M.D.; Manasova, M.; Rysanek, P.; Zouhar, M. Characterization of the Molecular Mechanisms of Resistance against DMI Fungicides in *Cercospora beticola* Populations from the Czech Republic. *J. Fungi* **2021**, *7*, 1062. [CrossRef] [PubMed]
22. Rolando, C.; Somchit, C.; Bader, M.K.-F.; Fraser, S.; Williams, N. Can Copper Be Used to Treat Foliar Phytophthora Infections in *Pinus radiata*? *Plant Dis.* **2019**, *103*, 1809–2147. [CrossRef] [PubMed]
23. Coque, J.J.R.; Álvarez-Pérez, J.M.; Cobos, R.; González-García, S.; Ibáñez, A.M.; Diez Galán, A.; Calvo-Peña, C. Advances in the control of phytopathogenic fungi that infect crops through their root system. *Adv. Appl. Microbiol.* **2020**, *111*, 123–170. [CrossRef] [PubMed]
24. Werres, S.; Marwitz, R.; Man In't veld, W.A.; De Cock, A.W.A.M.; Bonants, P.J.M.; De Weerdt, M.; Baayen, R.P. Phytophthora ramorum sp. nov., a new pathogen on Rhododendron and Viburnum. *Mycool. Res.* **2001**, *105*, 1155–1165. [CrossRef]
25. European Food Safety Authority. Peer review of the pesticide risk assessment of the active substance copper compounds copper(I), copper(II) variants namely copper hydroxide, copper oxychloride, tribasic copper sulfate, copper(I) oxide, Bordeaux mixture. *EFSA J.* **2018**, *16*, e05152. [CrossRef]
26. Nečas, D.; Klapetek, P. Gwyddion: An open-source software for SPM data analysis. *Centr. Eur. J. Phys.* **2012**, *10*, 181–188. [CrossRef]
27. Abbott, W.S. A Method of Computing the Effectiveness of an Insecticide. *J. Econ. Entomol.* **1925**, *18*, 265–267. [CrossRef]
28. Vinceković, M.; Topolovec Pintarić, S.; Jurić, S.; Viskić, M.; Jalšenjak, N.; Bujan, M.; Đermić, E.; Žutić, I.; Fabek, S. Release of *Trichoderma viride* Spores from Microcapsules Simultaneously Loaded with Chemical and Biological Agents. *Agric. Consp. Sci.* **2017**, *82*, 395–401.
29. Gamo, I. Infrared Absorption Spectra of Water of Crystallization in Copper Sulfate Penta- and Monohydrate Crystals. *Bull. Chem. Soc. Jpn.* **1961**, *34*, 764–766. [CrossRef]
30. Hu, C.; Lu, W.; Mata, A.; Nishinari, K.; Fang, Y. Ions-induced gelation of alginate: Mechanisms and applications. *Int. J. Biol. Macromol.* **2021**, *177*, 578–588. [CrossRef] [PubMed]
31. Jurić, S.; Đermić, E.; Topolovec-Pintarić, S.; Bedek, M.; Vinceković, M. Physicochemical properties and release characteristics of calcium alginate microspheres loaded with *Trichoderma viride* spores. *J. Integr. Agric.* **2019**, *18*, 2–16. [CrossRef]
32. Haug, A.; Smidsrod, O.A.; Högdahl, B.; Øye, H.A.; Rasmussen, S.E.; Sunde, E.; Sörensen, N.A. Selectivity of Some Anionic Polymers for Divalent Metal Ions. *Acta Chem. Scand.* **1970**, *24*, 843–854. [CrossRef]
33. De Souza, J.F.; Aquino, T.F.; Nascimento, J.E.; Jacob, R.G.; Fajardo, A.R. Alginate-copper microspheres as efficient and reusable heterogeneous catalysts for the one-pot synthesis of 4-organylselanyl-1H-pyrazoles. *Catal. Sci. Technol.* **2020**, *10*, 3918–3930. [CrossRef]
34. Rashedy, S.H.; Abd El Hafez, M.S.M.; Dar, M.A.; Cotas, J.; Pereira, L. Evaluation and Characterization of Alginate Extracted from Brown Seaweed Collected in the Red Sea. *Appl. Sci.* **2021**, *11*, 6290. [CrossRef]
35. Lu, L.; Liu, X.; Tong, Z. Critical exponents for sol–gel transition in aqueous alginate solutions induced. *Carbohydr. Polym.* **2006**, *65*, 544–551. [CrossRef]

36. Papageorgiou, S.K.; Kouvelos, E.P.; Favvas, E.P.; Sapalidis, A.A.; Romanos, G.E.; Katsaros, F.K. Metal–carboxylate interactions in metal–alginate complexes studied with FTIR Spectroscopy. *Carbohydr. Res.* **2010**, *345*, 469–473. [CrossRef] [PubMed]
37. Omidian, H.; Rocca, J.G.; Park, K. Advances in superporous hydrogels. *J. Control. Release* **2005**, *102*, 3–12. [CrossRef] [PubMed]
38. Jurić, S.; Šegota, S.; Vinceković, M. Influence of surface morphology and structure of alginate microparticles on the bioactive agents release behavior. *Carbohydr. Polym.* **2019**, *218*, 234–242. [CrossRef] [PubMed]
39. Xie, H.G.; Zheng, J.N.; Li, X.X.; Liu, X.D.; Zhu, J.; Wang, F.; Xie, W.Y.; Ma, X.J. Effect of surface morphology and charge on the amount and conformation of fibrinogen adsorbed onto alginate/chitosan microcapsules. *Langmuir* **2010**, *26*, 5587–5594. [CrossRef] [PubMed]
40. Roy, A.; Singh, S.K.; Bajpai, J.; Bajpai, J.K. Controlled pesticide release from biodegradable Polymers. *Cent. Eur. J. Chem.* **2014**, *12*, 453–469. [CrossRef]
41. Gray, A.; Egan, S.J.; Bakalis, S.; Zhang, Z. Determination of microcapsule physicochemical, structural, and mechanical properties. *Particuology* **2016**, *24*, 32–43. [CrossRef]
42. Cheng, W.; Dunn, P.F.; Brach, R.M. Surface roughness effects on microparticle adhesion. *J. Adhesion.* **2002**, *78*, 929–965. [CrossRef]
43. Leick, S.; Kott, M.; Degen, P.; Henning, S.; Päsler, T.; Suter, D.; Rehage, H. Mechanical properties of liquid-filled shellac composite capsules. *Phys. Chem. Chem. Phys. PCCP* **2011**, *13*, 2765–2773. [CrossRef] [PubMed]
44. Malektaj, H.; Drozdov, A.D.; de Claville Christiansen, J. Mechanical Properties of Alginate Hydrogels Cross-Linked with Multivalent Cations. *Polymers* **2023**, *15*, 3012. [CrossRef] [PubMed]
45. Siepmann, J.; Siepmann, F. Modeling of diffusion controlled drug delivery. *J. Control. Release* **2012**, *161*, 351–362. [CrossRef] [PubMed]
46. Vinceković, M.; Jurić, S.; Đermić, E.; Topolovec Pintarić, S. Kinetics and Mechanisms of Chemical and Biological Agents Release from Biopolymeric Microcapsules. *J. Agric. Food Chem.* **2017**, *65*, 9608–9617. [CrossRef] [PubMed]
47. Talevi, A.; Ruiz, M.E. Korsmeyer-Peppas, Peppas-Sahlin, and Brazel-Peppas: Models of Drug Release. In *The ADME Encyclopedia*; Springer: Cham, Switzerland, 2021; pp. 1–9. [CrossRef]
48. Vigata, M.; Meinert, C.; Hutmacher, D.W.; Bock, N. Hydrogels as Drug Delivery Systems: A Review of Current Characterization and Evaluation Techniques. *Pharmaceutics* **2020**, *12*, 1188. [CrossRef] [PubMed]
49. Mularczyk-Oliwa, M.; Bombalska, A.; Kaliszewski, M.; Włodarski, M.; Kwaśny, M.; Kopczyński, K.; Szpakowska, M.; Trafny, E.A. Rapid discrimination of several fungus species with FTIR spectroscopy and statistical analysis. *Biul. Wojsk. Akad. Tech.* **2013**, *62*, 71–80.
50. Salman, A.; Pomerantz, A.; Tsror, L.; Lapidot, I.; Moreh, R.; Mordechai, S.; Huleihel, M. Utilizing FTIR-ATR spectroscopy for classification and relative spectral similarity evaluation of different *Colletotrichum coccodes* isolates. *Analyst* **2012**, *137*, 3558–3564. [CrossRef] [PubMed]
51. Skolik, P.; Morais, C.L.M.; Martin, F.L.; McAinsh, M.R. Attenuated total reflection Fourier-transform infrared spectroscopy coupled with chemometrics directly detects pre- and post-symptomatic changes in tomato plants infected with *Botrytis cinerea*. *Vib. Spectrosc.* **2020**, *111*, 103171. [CrossRef]
52. Wittayapipath, K.; Laolit, S.; Yenjai, C.; Chio-Srichan, S.; Pakarasang, M.; Tavichakorntrakool, R.; Prariyachatigul, C. Analysis of xanthyletin and secondary metabolites from *Pseudomonas stutzeri* ST1302 and *Klebsiella pneumoniae* ST2501 against *Pythium insidiosum*. *BMC Microbiol.* **2019**, *19*, 78. [CrossRef] [PubMed]
53. Salman, A.; Lapidot, I.; Pomerantz, A.; Tsror, L.; Shufan, E.; Moreh, R.; Mordechai, S.; Huleihel, M. Identification of fungal phytopathogens using Fourier transform infrared-attenuated total reflection spectroscopy and advanced statistical methods. *J. Biomed. Opt.* **2012**, *17*, 017002. [CrossRef]
54. Szeghalmi, A.; Kaminskyj, S.; Gough, K.M. A synchrotron FTIR microspectroscopy investigation of fungal hyphae grown under optimal and stressed conditions. *Anal. Bioanal. Chem.* **2007**, *387*, 1779–1789. [CrossRef] [PubMed]
55. Synytsya, A.; Novak, M. Structural analysis of glucans. *Ann. Transl. Med.* **2014**, *2*, 17. [CrossRef] [PubMed]
56. Pei, Y.; Tao, Q.J.; Zheng, X.; Li, Y.; Sun, X.; Li, Z.; Gong, G. Phenotypic and Genetic Characterization of *Botrytis cinerea* Population from Kiwifruit in Sichuan Province, China. *Plant Dis.* **2019**, *103*, 748–758. [CrossRef] [PubMed]
57. Oerke, E.C.; Leucker, M.; Steiner, U. Sensory assessment of *Cercospora beticola* sporulation for phenotyping the partial disease resistance of sugar beet genotypes. *Plant Methods* **2019**, *15*, 133. [CrossRef] [PubMed]
58. Grünwald, N.J.; Goss, E.M.; Press, C.M. *Phytophthora ramorum*: A pathogen with a remarkably wide host range causing sudden oak death on oaks and ramorum blight on woody ornamentals. *Mol. Plant Pathol.* **2008**, *9*, 729–740. [CrossRef] [PubMed]
59. Ghosh, S.; Rusyn, I.; Dmytruk, O.V.; Dmytruk, K.V.; Onyeaka, H.; Gryzenhout, M.; Gafforov, Y. Filamentous fungi for sustainable remediation of pharmaceutical compounds, heavy metal and oil hydrocarbons. *Front. Bioeng. Biotechnol.* **2023**, *11*, 1106973. [CrossRef] [PubMed]
60. Gow, N.A.R.; Lenardon, M.D. Architecture of the dynamic fungal cell wall. *Nat. Rev. Microbiol.* **2023**, *21*, 248–259. [CrossRef]
61. McGowan, J.; Fitzpatrick, D.A. Chapter Five—Recent advances in comycete genomics. *Adv. Genet.* **2020**, *105*, 175–228. [CrossRef] [PubMed]
62. Dusengemungu, L.; Kasali, G.; Gwanama, C.; Ouma, K.O. Recent Advances in Biosorption of Copper and Cobalt by Filamentous Fungi. *Front. Microbiol.* **2020**, *11*, 582016. [CrossRef] [PubMed]

63. Jurić, S.; Tanuwidjaja, I.; Fuka, M.M.; Vlahoviček-Kahlina, K.; Marijan, M.; Boras, A.; Kolić, N.U.; Vinceković, M. Encapsulation of two fermentation agents, *Lactobacillus sakei* and calcium ions in microspheres. *Colloids Surf. B* **2021**, *197*, 111387. [CrossRef] [PubMed]
64. Wargenau, A.; Fleissner, A.; Bolten, C.J.; Rohde, M.; Kampen, I.; Kwade, A. On the origin of the electrostatic surface potential of *Aspergillus niger* spores in acidic environments. *Res. Microbiol.* **2011**, *162*, 1011–1017. [CrossRef] [PubMed]
65. Dunlap, C.A.; Biresaw, G.; Jackson, M.A. Hydrophobic and electrostatic cell surface properties of blastospores of the entomopathogenic fungus *Paecilomyces fumosoroseus*. *Colloids Surf. B Biointerfaces* **2005**, *46*, 261–266. [CrossRef] [PubMed]
66. Wu, X.; Liu, J.; Liu, Z.; Gong, G.; Zha, J. Microbial cell surface engineering for high-level synthesis of bio-products. *Biotechnol. Adv.* **2022**, *55*, 107912. [CrossRef] [PubMed]
67. Vasina, D.V.; Antonova, N.P.; Shidlovskaya, E.V.; Kuznetsova, N.A.; Grishin, A.V.; Akoulina, E.A.; Trusova, E.A.; Lendel, A.M.; Mazunina, E.P.; Kozlova, S.R.; et al. Alginate Gel Encapsulated with Enzybiotics Cocktail Is Effective against Multispecies Biofilms. *Gels* **2024**, *10*, 60. [CrossRef] [PubMed]
68. Vicedo, B.; de la O Leyva, M.; Flors, V.; Finiti, I.; Del Amo, G.; Walters, D.; Real, M.D.; García-Agustín, P.; González-Bosch, C. Control of the phytopathogen *Botrytis cinerea* using adipic acid monoethyl ester. *Arch. Microbiol.* **2006**, *184*, 316–326. [CrossRef] [PubMed]
69. Rodríguez-Ramos, F.; Briones-Labarca, V.; Plaza, V.; Castillo, L. Iron and copper on *Botrytis cinerea*: New inputs in the cellular characterization of their inhibitory effect. *PeerJ* **2023**, *11*, e15994. [CrossRef] [PubMed]
70. Liu, H.F.; Xue, X.J.; Yu, Y.; Xu, M.M.; Lu, C.C.; Meng, X.L.; Zhang, B.G.; Ding, X.H.; Chu, Z.H. Copper ions suppress abscisic acid biosynthesis to enhance defence against *Phytophthora infestans* in potato. *Mol. Plant Pathol.* **2020**, *21*, 636–651. [CrossRef] [PubMed]
71. Xue, W.M.; Yu, W.T.; Liu, X.D.; He, X.; Wang, W.X.; Ma, J. Chemical method of breaking the cell-loaded sodium alginate/chitosan microcapsules. *Chem. J. Chin. Univ.* **2004**, *25*, 1342–1346. Available online: http://www.cjcu.jlu.edu.cn/EN/Y2004/V25/I7/1342 (accessed on 16 July 2022).
72. Mokale, V.; Jitendra, N.; Yogesh, S.; Gokul, K. Chitosan reinforced alginate controlled release beads of losartan potassium: Design, formulation and in vitro evaluation. *J. Pharm. Investig.* **2014**, *44*, 243–252. [CrossRef]